Design of Pedal Bicycle Prototype using the PID Controller as an Alternative Energy Generator

Rizanty Reyhan[1], Efendi S Wirateruna[2]*, Anang Habibi[3]
[1,2,3]Electrical Engineering, Faculty of Engineering, University of Islam Malang, Indonesia
[1]21901053010@unisma.ac.id; [2*]efendi.s.wirateruna@unisma.ac.id ; [3]ananghabibi@unisma.ac.id
*corresponding author

ABSTRACT

In recent years, electricity consumption in Indonesia rose to 1.109 kWh, as the Ministry of Energy and Mineral Resources reported. An alternate method for generating electrical energy is harvesting the energy produced via exercising on a stationary bike. By employing Arduino Mega 2560pro-powered torque control using the PID (Proportional – Integral – Derivative) technique, we can effectively save the generator's power in the battery and modify the paddle load to match the user's desired settings. The design incorporates a repurposed bicycle that has been rebuilt, along with the addition of a transmission gear, a controller box housing a control circuit, a relay, and an inverter. Additionally, it is equipped with a display and buttons. This system can generate a paddle load ranging from 1 to 17 in normal mode and 1 to 10 in PID mode. The system has a maximum current output of 3.2A and a battery capacity of 24VDC. This DC voltage is then transformed into a 220 VA AC voltage suitable for residential electrical use using an inverter. The PID controller will regulate the current flowing into the battery, ensuring it remains steady even with a consistent wood load. PID control can reach a set point at the settling time, 7 s, with an overshoot and a steady-state error of 0%. Every motor achieved the Pulse Width Modulation (PWM) value set to the ideal current. As the RPM increases, the PWM decreases until it reaches the preset set point with a constant current value.

Keywords: Keywords: Bicycle; Renewable Energy; PID Controller; Arduino; Generator.

Article History

Received : Jan, 27th 2024	Accepted : May, 30th 2024	Published : Jun, 06th 2024

I. INTRODUCTION

Presently, electrical energy generation in Indonesia predominantly depends on non-renewable sources, particularly coal fuel. As a result, there is a potential danger that the availability of this energy source may someday run out. According to the Ministry of Energy and Natural Resources, the expected increase in power consumption per individual is up to 1,109 kWh by September 2021 [1], [2]. Several ongoing programs aim to develop alternatives that ensure the availability of electrical energy despite the depletion of natural resources [3]. Renewable energy is an alternative that aims to maximize the production of electricity [4], [5], [6]. The energy sources for generating electricity include renewable resources such as solar power, wind power, geothermal energy, and water [7], [8]. Renewable energy can be obtained from both primary natural resources and physical material resources, including gravity, pressure, mechanical energy, and kinetic energy [7], [9], [10], [11], [12], [13].

Implementing renewable energy sources in technological breakthroughs would optimize human activity while fostering environmental sustainability. Individuals can achieve this consciousness by regularly participating in physical activities like exercise. Cycling is presently a widely favoured athletic pursuit among individuals. Participating in long-distance cycling can consume calories and generate inspiration [14]. Nevertheless, if the bicycle is fitted with a permanent magnetic generator, the mechanical energy produced by pedalling can be converted into electrical energy [9], [15], [16]. Thus, bicycles in static mode can produce self-electricity as a renewable energy alternative [17]. There is potential for development to optimize energy harvesting as static technology [6], [18], [19].

A static bike is electrically powered sporting equipment designed to reduce the need for physical exertion while being environmentally friendly. Exercises on a stationary bike can be done irrespective of weather conditions, anytime and anywhere. The generated electrical energy can also be used for household electricity needs. In this article, a static bike was designed as other alternative sports equipment producing energy. A proportional-–integral–derivative (PID) controller was implemented to optimize the power output produced by mechanical energy from the wheel rotation of a static bike.

DOI: http://dx.doi.org/10.25139/ijair.v6i1.7761

E - ISSN : 2686-6269

II. METHOD

A. Block Diagram

Static bikes are the primary components that generate and convert kinetic energy into electrical energy. Fig.1 illustrates converting electricity generated by the generator into direct current (DC) using a rectifier diode. Current and voltage sensors measure the electrical current and voltage generated. There are three current and voltage sensors positioned at different locations. The permanent current and voltage sensors are positioned upstream of the PWM signal circuit to guarantee the unidirectional / DC nature of the generated current from the generator. After manipulating the PWM signal, the second sensor is positioned upstream of the battery. At this point, the current and voltage will be assessed to determine their compatibility with the desired output power setpoint before being sent to the battery. The third current sensor is incorporated with a relay linked to an inverter. This positioning guarantees that the output power is suitable and may be transformed into alternating current (AC). The battery has a voltage capacity 12V×2, connected in series to achieve a total voltage storage of 24V. The relay may be engaged via the button on the display, allowing the user to control the battery usage based on their preferences. The third voltage sensor is positioned downstream of the inverter to enable the LCD to display the voltage intended for the load.

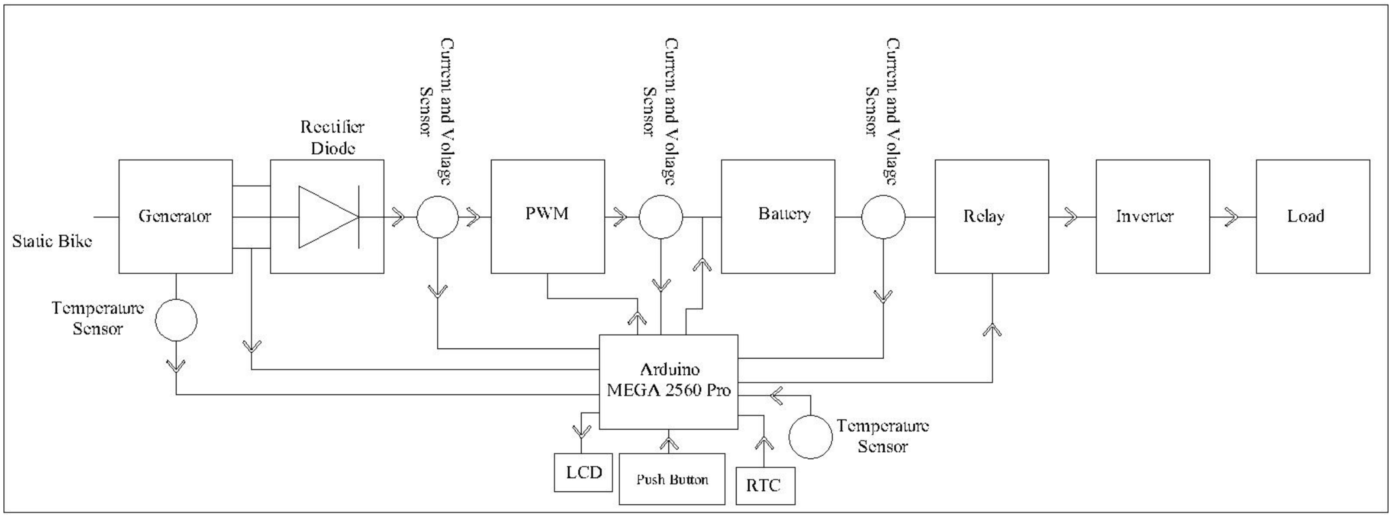

Fig.1. Block Diagram System

The Arduino MEGA250 microcontroller is the primary controller for manipulating the PWM signal. Additionally, it is responsible for controlling the input and output components inside the system. The system's input comprises a generator, current and voltage sensors, temperature sensor, push button, and RTC. The system's output comprises PWM, LCD, and relay signals. The display box is equipped with push buttons and LCDs, allowing the presentation of several menus. These menus include user information, generator, battery status, and day and time display. Each button is assigned specific instructions to control the shown information. The push button comprises three distinct buttons: menu, up, and down. The purpose of the menu button is to present information, while the up and down buttons are utilized for torque control. The LCD will display the temperature sensor and RTC readings. In contrast, the current and voltage sensor readings will display the power or electrical energy generated, which will also be shown on the LCD.

B. Research Flow Diagram

This section presents the research steps depicted in Fig.2, which include examining existing literature, formulating the system design, and gathering data from the system's test components, including sensors. Once the sensor undergoes testing, it proceeds to calculate the Mean Absolute Percentage Error (MAPE) [20], [21]. Suppose the average error value achieved is less than or equal to 5%. In that case, the further steps include developing a stationary bicycle system, programming a microcontroller, conducting system testing, and analyzing the test findings. MAPE using Equation (1). The *N* variable is a number of values, the A_i variable is real values, and the F_i variable is approximate values.

$$MAPE = \frac{1}{n} \sum \genfrac{}{}{0pt}{}{N}{i} = 1 \frac{|Ai - Fi|}{Ai} \times 100 \qquad (1)$$

DOI: http://dx.doi.org/10.25139/ijair.v6i1.7761

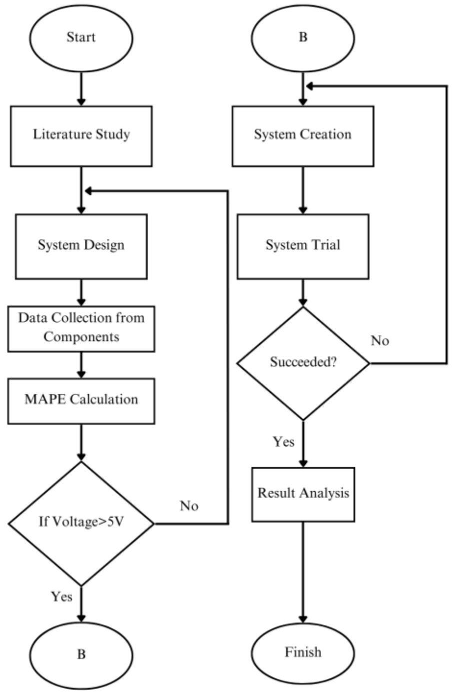

Fig.2. Research Flow Diagram

C. *Software Block Diagram*

Fig.3 explains the illustration: when the system starts, the LCD will automatically turn on, and a buzzer will sound, indicating that the system is on standby and can be used. After that, the Arduino will read the RTC, current, voltage, and temperature sensor values.

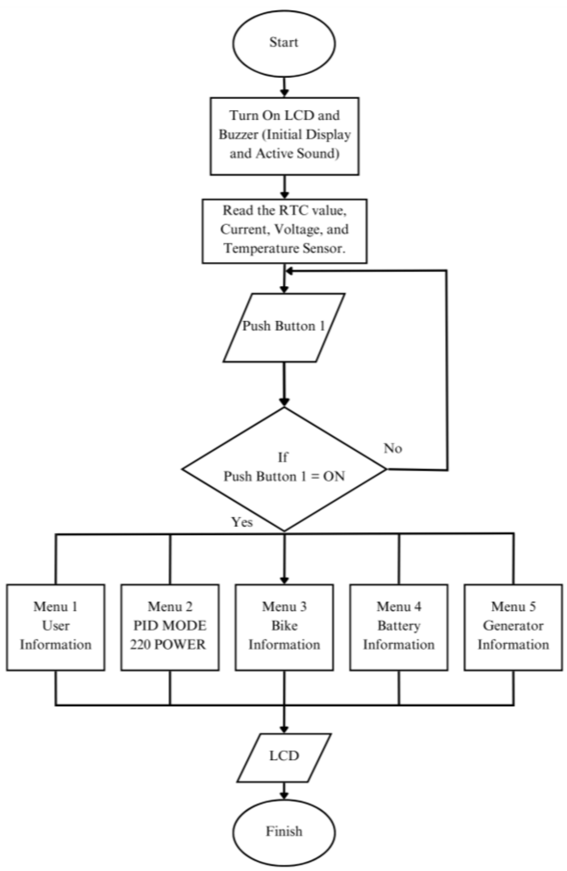

Fig.3. System Flow Diagram

DOI: http://dx.doi.org/10.25139/ijair.v6i1.7761

 E - ISSN : 2686-6269

When push button 1 is pressed once, menu 1 will appear on the LCD containing user information, and the user can customize the torque. When push button 1 is pressed a second time, menu 2 will appear on the LCD, which contains information regarding PID mode and power 220 on-off, which can be used as a backup power source at home. When button 1 is pressed the third time, menu 3 will appear on the LCD, which contains bicycle information such as current torque, room temperature, and power produced. When push button 1 is pressed the fourth time, menu 4 will appear, displaying battery information such as the current produced, voltage, and power used when the battery is used. When button 1 is pressed the fifth time, menu 5 will appear, displaying generator information containing current, voltage, and temperature.

A. System Sequence

The isolated power supply circuit comprises the PWM amplifier and 30kHz pulse-generating circuits. The Arduino microcontroller will generate the PWM signal via the PWM amplifier circuit. Subsequently, the signal will be directed to the power transistor (IRFP250) and regulated by the driver (optocoupler 6N137 and transistor BD140). The circuit for the pulse generator operating at a frequency of 30kHz will deliver a voltage supply to the power transistor driver. The relay circuit will trigger the inverter, allowing the battery's stored voltage to be utilized for domestic electricity at a level of 220V. The buck-boost range is intended to provide a 5V voltage supply for the Arduino microcontroller, ACS712 Sensor, Op-Amp CA3130, and IC555, using power from the battery. A component circuit is an electrical circuit that includes input/output combinations of voltage, current, and temperature sensors, as depicted in Fig.4.

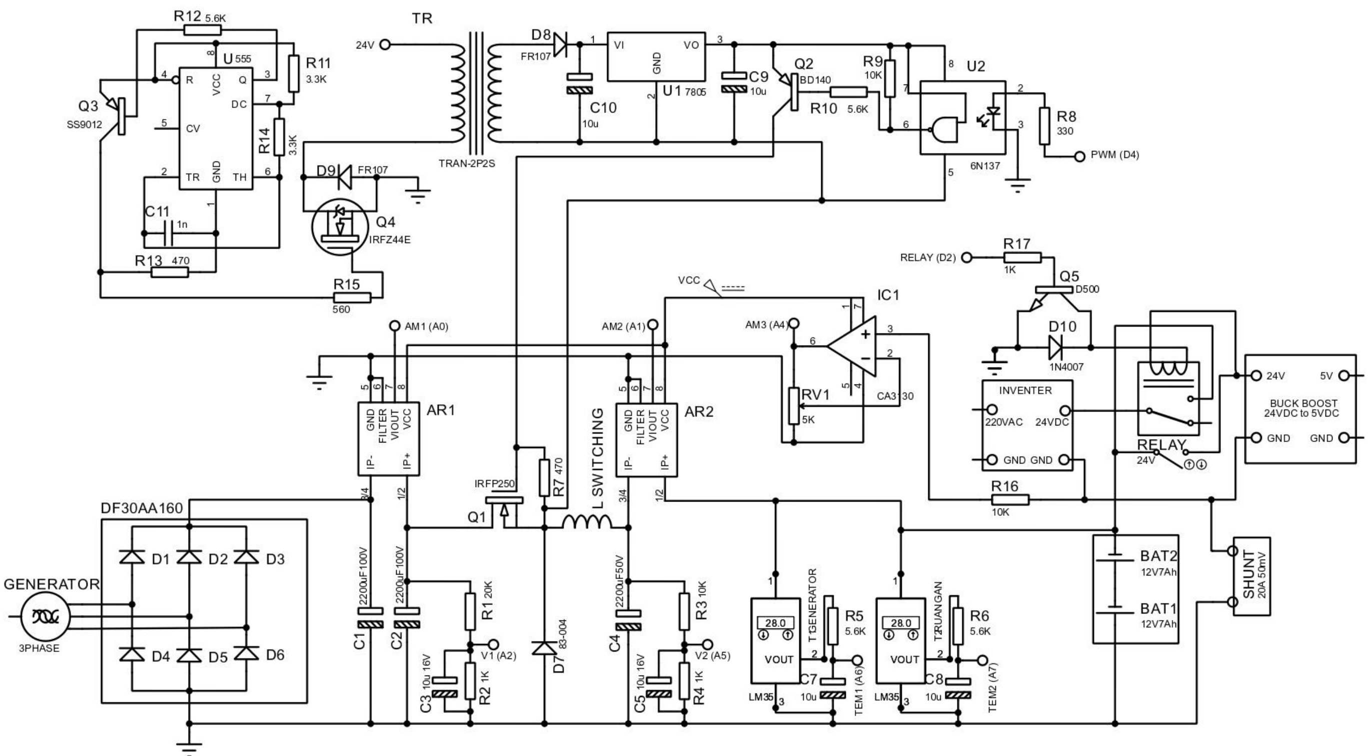

Fig.4. System Sequence

III. RESULT AND DISCUSSION

A. Bicycle System

Fig.5 depicts a series of stationary bicycles. The design of the bicycle gearbox system in these bicycles aims to control the rotating motion of the generator. The gearbox system comprises substantial gears, diminutive gears, and sizable and petite pulleys. They are positioned at the front of the bicycle. Small pulleys rotate the generator, and the resulting AC to DC energy conversion is transmitted through the cabling on the bicycle body to the box panel behind the bicycle. The box panel houses a set of controllers, relays, and inverters.

DOI: http://dx.doi.org/10.25139/ijair.v6i1.7761

 E - ISSN : 2686-6269

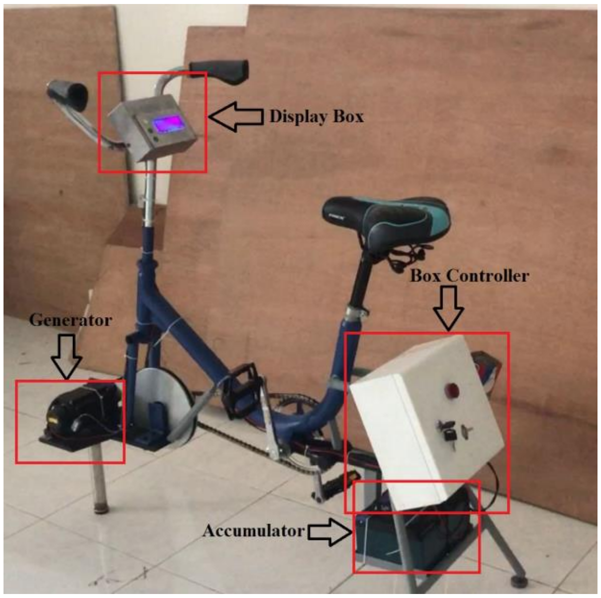

Fig.5. Bicycle System

B. Tool Circuit

The tool circuit has many components, as depicted in Figure 6, including a voltage generator for powering the system. The Acs712 current sensor measures the current produced by the generator and the current flowing into the battery. The voltage multiplier circuit is used to quantify the current flowing from the battery to the inverter. There are two DC voltage sensors, each having a distinct purpose. One sensor originating from the generator's voltage output is utilized to measure the voltage that will be supplied to the Arduino. The other sensor measures the voltage that will be stored in the battery. The Arduino Mega2560 Pro serves as the central control unit of the system. The step-up buck converter is responsible for precisely increasing the voltage to 24 volts. A 16x4 I2C LCD is used to show the sensors' readings. These sensors are connected to an Arduino 2560 Mega.


Fig.6. Tool circuit

C. Voltage Sensor Test

Table I shows the results and calculation of the voltage sensor measured using a sensor that shows results close to the voltage measured using a multimeter with a MAPE value of 1.16%. Because the MAPE value obtained is by the design, namely MAPE ≤ 5%, the test is continued to the battery voltage sensor test.

TABLE I
Test Results and Calculation of Generator Voltage Sensor

Multimeter Voltage (V)	Sensor Voltage (V)	MAPE (%)
5.12	5.04	1.5
25.14	24.74	1.6
75.23	74.93	0.4
Mean Absolute Percentage Error (MAPE)		1,16

Table II explains that the voltage measured using a sensor shows results close to that measured using a multimeter with a MAPE value of 1.23%. Because the MAPE value obtained is by design, namely MAPE ≤ 5%, the test is continued to the next component test.

DOI: http://dx.doi.org/10.25139/ijair.v6i1.7761

 E - ISSN : 2686-6269

TABLE II
Test Results and Calculation of Battery Voltage Sensor

Multimeter Voltage (V)	Sensor Voltage (V)	MAPE (%)
5.07	4.97	1.9
25.53	25.31	0.8
50.09	50.6	1
Mean Absolute Percentage Error (MAPE)		1,23

D. Current Sensor Test

Table III illustrates that the current detected by the ACS712 sensor at 0.5A, 1A, 1.5A, and 2A is nearly identical to the current measured by a multimeter. Nevertheless, it remains imperative to perform an error computation. The results obtained from the error computation are presented in Table III. Therefore, since the final calculated MAPE is 1.05%, which is within the specified design limit of MAPE ≤ 5%, it may be concluded that the sensor is in good condition and can be utilized.

TABLE III
Test Results and Calculation of ACS712 Sensor

Multimeter Current (A)	Sensor Current (A)	MAPE (%)
0.51	0.50	1.2
1.03	1.02	0.78
1.54	1.53	0.68
2.07	2.04	1.55
Mean Absolute Percentage Error (MAPE)		1.05

Table IV demonstrates that the current obtained by a voltage multiplier circuit, ranging from 1A to 5A, is nearly identical to the current measured with a multimeter. Nevertheless, it remains imperative to perform an error computation. The outcome is acquired and presented in Table IV upon completion of the error calculation. Specifically, the final calculation yields a Mean Absolute Percentage Error (MAPE) of 1.5%. Since the obtained MAPE adheres to the specified design criterion of MAPE ≤ 5%, the sensor can be deemed suitable for operation under optimal conditions.

TABLE IV
Test Results and Calculation of Voltage Multiplier Circuit

Multimeter Current (A)	Sensor Current (A)	MAPE (%)
1.01	1.00	1.2
2.11	2.08	1.4
3.09	3.03	2
4.24	4.22	0.6
5.08	5.20	2.3
Mean Absolute Percentage Error (MAPE)		1.5

E. PID System Diagram

PID controller is the most popular control used to optimize energy[22], [23], [24], [25]. As shown in Fig.7, the PID system diagram is based on a diagram of a closed control system where the sensor reading process becomes constant feedback, and the calculation of the desired actuator output is repeated continuously so that it reaches the set point in this system is the amount of the torque desired by the user.

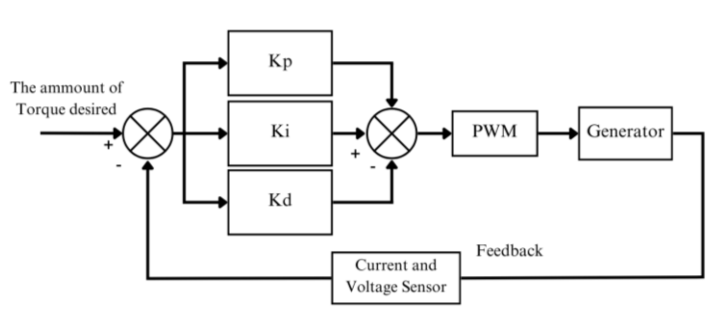

Fig.7. PID System Diagram

F. System Testing

System testing is conducted to evaluate the performance of the PID control system design on the static bicycle design. To begin, gather the essential tools: a fully assembled bicycle, the Arduino IDE with a serial program capable of transmitting PWM data and current to a laptop, and a tachometer for measuring RPM during testing. Testing was conducted on five distinct torque scales, resulting in a ratio of 17:5 for the normal mode, as indicated in Table V. As indicated in Table V, the torque in normal mode that was taken for the testing is only 5 torque of 17 total of torque, which is torque 3, torque 6, torque 9, torque 13, and torque 15.

TABLE V
Normal Mode Torque Test Sample

Torque	PWM	Duty Cycle (%)
3	45	17.58

DOI: http://dx.doi.org/10.25139/ijair.v6i1.7761

E - ISSN : 2686-6269

Torque	PWM	Duty Cycle (%)
6	89	34.77
9	135	52.73
13	195	76.17
15	225	87.89

Testing is conducted on five distinct torque scales in PID Mode, with a ratio of 10:5. The PID data includes the ACS value and the current value, which are obtained from calculations in the program, as depicted in Table VI. As the duty cycle increases, the user experiences a larger sensation of weight in the paddle.

TABLE VI
PID Mode Torque Test Sample

Torque	PID Data	
	ACS	Current (A)
2	2.79	0.56
4	5.58	1.12
6	8.38	1.68
8	11.17	2.24
10	13.96	2.80

Sensor reading results for the PID technique and without PID will be analyzed through Fig.8 and Fig.9. For comparison, the torque is varied. Figure 8 displays the RPM-to-current ratio in the battery during normal mode, using torque values of 3, 6, 9, 13, 15, and 17 on the scale. The graph illustrates a positive correlation between the magnitude of RPM (the bicycle stroke rate) and the generated current. At torque level 3, when the revolutions per minute (RPM) reaches 1740, the maximum current generated is 0.6 Amperes (A). At a torque of 6, when the revolutions per minute (RPM) reaches 1740, the maximum current generated is 1.2A. The highest current generated when the RPM hits 1740 at torque 9 is 1.8A. When the torque is set to 13, the maximum current generated is 2.4A at an RPM of 1740. When the torque is set to 15 and the RPM hits 1740, the maximum current generated is 2.8A. When the torque is set at 17, and the RPM hits 1740, the maximum current generated is 3.2A. Based on the graph in Fig. 8, the maximum current can be predicted if the torque is higher than 17. It should be more than 3.5 A. In this paper, the maximum torque implemented is 17. The maximum current varies for each torque due to adjusting the PWM value on each scale, resulting in a distinct paddle load.

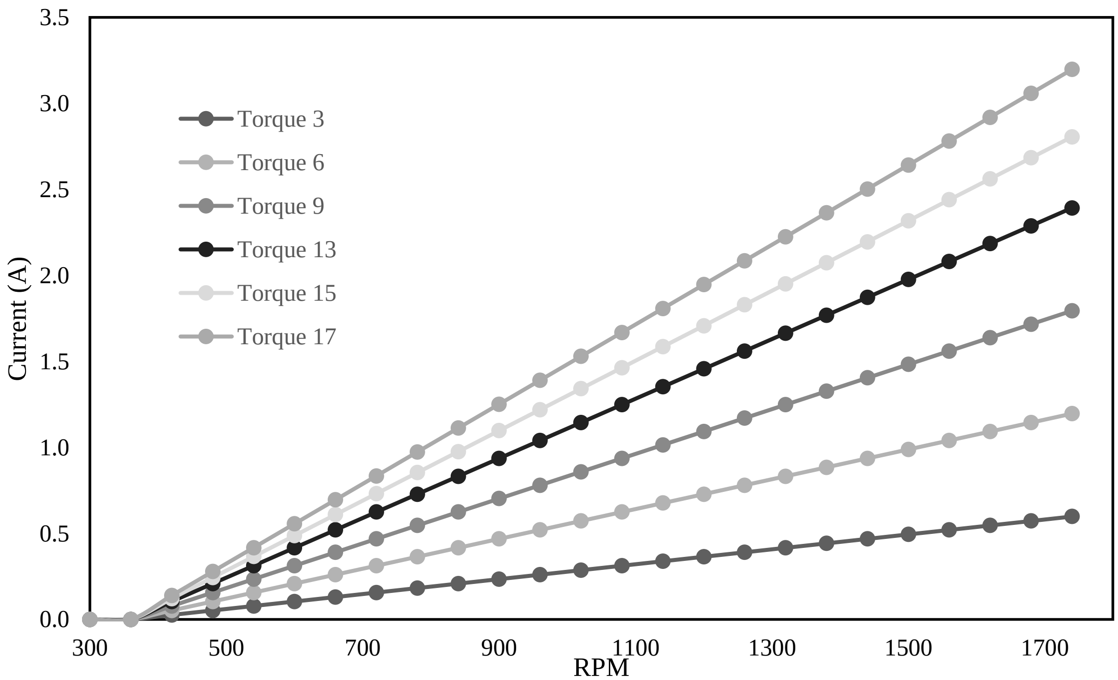

Fig.8. RPM-to-Current Ratio in Normal Mode

Figure 9 compares RPM and PWM in normal mode, specifically on the 3, 6, 9, 13, 15, and 17 torque scales. The graph illustrates that the PWM value will remain consistent despite increased RPM (bicycle). There are 3 pulse-width modulation (PWM) signals with a frequency of 45. The duty cycle for each signal is set at 18%. The torque of 89 is achieved with a 35% duty cycle using 6 PWM. The torque of 9 PWM is 135 when the duty cycle is 53%. The torque 195 is achieved with a 76% duty cycle using 13 PWM. The torque of 225 is achieved with a duty cycle of 88% using a 15 PWM signal. The torque of 254 is achieved by applying a Pulse Width Modulation (PWM) signal with a duty cycle of 99%.

 E - ISSN : 2686-6269

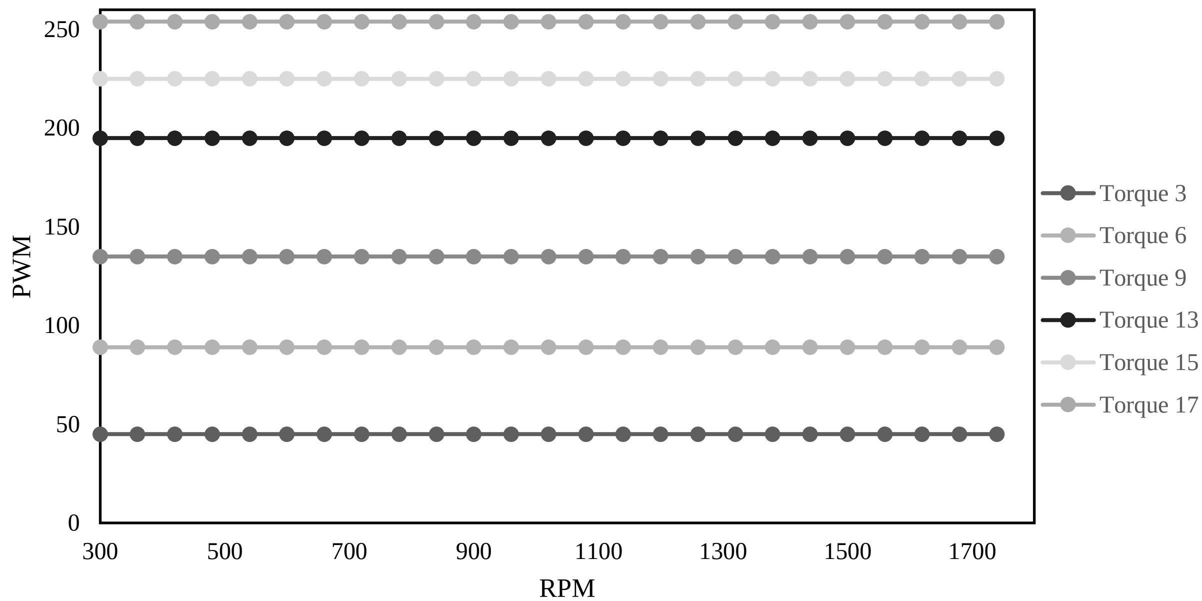

Fig.9. RPM Graph Against PWM Normal Mode

Fig.10 displays the RPM-to-current ratio when the PID mode is enabled on torque scales of 2.4, 6, 8, and 10. Two sets of torque values are getting tested because if we take one set, the results seen on the graph will not show a significant change, and the maximum torque in this mode is 10. If we want to take 5 samples, we just divide 10 and 5 until we get the difference in 2 sets. The graph illustrates that when the bicycle pedal's RPM (rotations per minute) increases, the generated current also increases. However, once the current reaches a specific threshold, it remains stable despite further changes in the bicycle pedal.

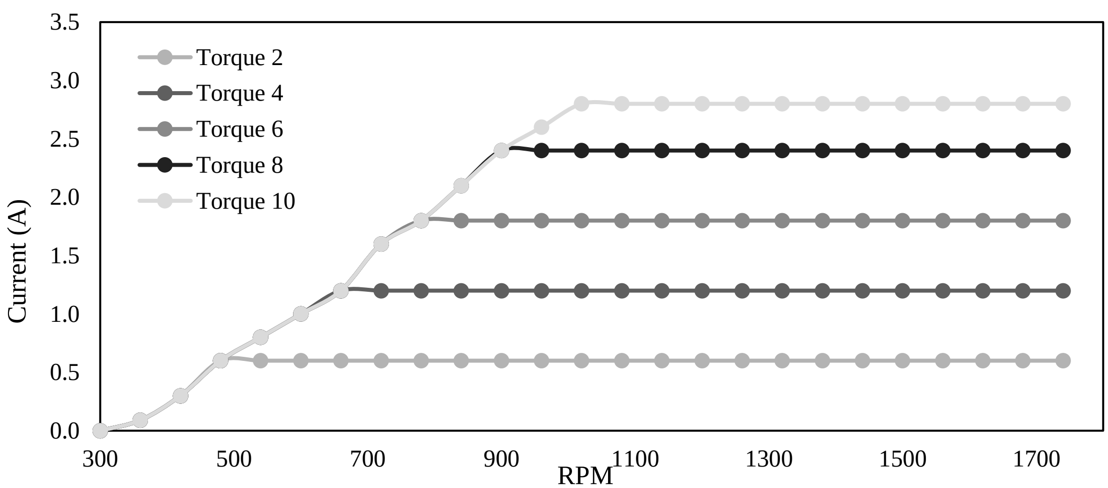

Fig.10. RPM-to-Current at Ratio in PID Mode

The observed phenomenon results from the implementation of PID control on PWM. Fig.11 illustrates the relationship between RPM and PWM when the PID mode is enabled, specifically for 2, 4, 6, 8, and 10 torque values. The graph illustrates that as the RPM increases (indicating a quicker bike ride), there is a corresponding decrease in the PWM value at a specific threshold. When the RPM reaches 480 and continues to grow, the current produced will remain constant at a maximum of 0.6A. This is achieved by reducing the PWM until it reaches a value of 45 or a duty cycle of 17%. At 4 amperes, the torque achieves its maximum value of 1.2A. As the RPM increases beyond 660, the current produced will remain constant. This is achieved by gradually reducing the PWM until it hits a value of 89 or a duty cycle of 35%. When the RPM reaches 780 and continues to grow, the current produced will remain constant at a maximum torque of 6 currents, generated by a current of 1.8A. This is achieved by reducing the PWM until it achieves a value of 135 or a duty cycle of 53%. At a torque of 8, the maximum current produced is 2.4A. The current value produced will remain constant as the RPM increases from 900 and beyond. This is achieved by reducing the PWM until it achieves a value of 195 or a duty cycle of 76%. When the RPM reaches 1020 and continues to grow, the current produced will remain constant at a maximum torque of 9 currents generated by 2.8A. This is achieved by reducing the PWM until it achieves a value of 225 or a duty cycle of 88%.

DOI: http://dx.doi.org/10.25139/ijair.v6i1.7761

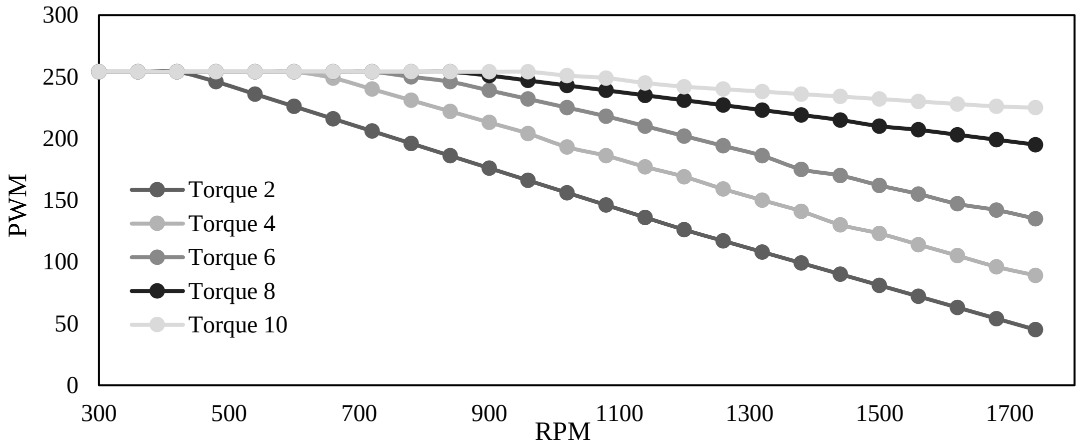

Figure 11 RPM Graph Against PWM PID Mode

The performance of PID control shown in Figure 12 explains that PID control can reach a set point at the settling time, 7 s, with overshoot and steady-state error 0%. It can be concluded that PID mode shows good performance in maintaining the current at the set point, 0,6 A.

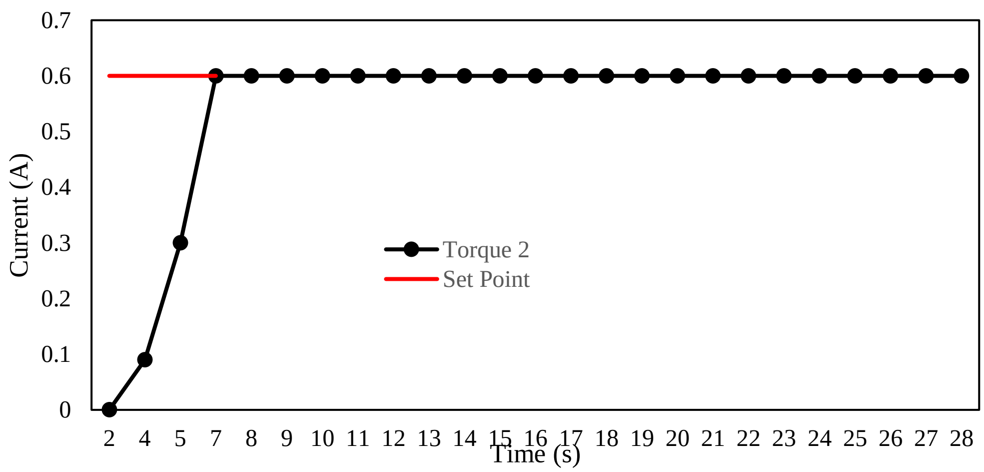

Fig.12. RPM Graph Against Time PID Mode

IV. CONCLUSION

The outcomes of this system evaluation pertain to the implementation of PID control to regulate the current flow into the battery. According to the conducted testing, this tool effectively measures the voltage the generator produces as it enters the Arduino and the voltage stored in the battery. The tool has a margin of error of 1.16% and 1.23%, respectively. This tool can accurately measure the current produced by the generator and the current flowing into the battery. It utilizes the ACS712 Sensor with a precision error rate of 1.05%.

Furthermore, the instrument can measure the electric current flowing from the battery to the inverter. A voltage multiplier circuit ensures no more than a 1.5% error rate. The LM35 temperature sensor, employed for measuring room temperature and generator temperature, exhibits an error margin of up to 0.90%, which remains within acceptable limits. According to the torque tests conducted on 2.4, 6, 8, and 10, this instrument effectively measures the generated current and achieves stability through PID control. The system's performance shows that PID control can reach a set point at the settling time, 7 s, with overshoot and steady-state error 0%. It can be concluded that PID mode shows good performance in maintaining the current at the set point, 0,6 A.

REFERENCES

[1] D. V. A., "Konsumsi Listrik Per Kapita Indonesia Capai 1.109 kWH pada Kuartal III 2021," https://databoks.katadata.co.id/datapublish/2021/12/10/konsumsi-listrik-per-kapita-indonesia-capai-1109-kwh-pada-kuartal-iii-2021.

[2] D. Hartono, S. H. Hastuti, A. A. Balya, and W. Pramono, "Modern energy consumption in Indonesia: Assessment for accessibility and affordability," *Energy for Sustainable Development*, vol. 57, pp. 57–68, 2020, doi: https://doi.org/10.1016/j.esd.2020.05.002.
[3] O. O. Yolcan, "World energy outlook and state of renewable energy: 10-Year evaluation," *Innovation and Green Development*, vol. 2, no. 4, p. 100070, 2023, doi: https://doi.org/10.1016/j.igd.2023.100070.
[4] Y. Majeed *et al.*, "Renewable energy as an alternative source for energy management in agriculture," *Energy Reports*, vol. 10, pp. 344–359, 2023, doi: https://doi.org/10.1016/j.egyr.2023.06.032.
[5] T.-Z. Ang, M. Salem, M. Kamarol, H. S. Das, M. A. Nazari, and N. Prabaharan, "A comprehensive study of renewable energy sources: Classifications, challenges and suggestions," *Energy Strategy Reviews*, vol. 43, p. 100939, 2022, doi: https://doi.org/10.1016/j.esr.2022.100939.
[6] A. Cicchella, "Human Power Production and Energy Harvesting," *Encyclopedia*, vol. 3, no. 2, pp. 698–704, 2023, doi: 10.3390/encyclopedia3020050.
[7] M. Ozcan, "The role of renewables in increasing Turkey's self-sufficiency in electrical energy," *Renewable and Sustainable Energy Reviews*, vol. 82. Elsevier Ltd, pp. 2629–2639, Feb. 01, 2018. doi: 10.1016/j.rser.2017.09.111.
[8] G. M. Masters, "Renewable and Efficient Electric Power Systems."
[9] S. Dubey, A. Sharma, V. K. Panchariya, M. K. Goyal, R. Y. Surampalli, and T. C. Zhang, "Regional sustainable development of renewable natural resources using Net Primary Productivity on a global scale," *Ecol Indic*, vol. 127, p. 107768, 2021, doi: https://doi.org/10.1016/j.ecolind.2021.107768.
[10] E. Kabir, P. Kumar, S. Kumar, A. A. Adelodun, and K.-H. Kim, "Solar energy: Potential and future prospects," *Renewable and Sustainable Energy Reviews*, vol. 82, pp. 894–900, 2018, doi: https://doi.org/10.1016/j.rser.2017.09.094.
[11] A. Sayigh, "Up-date: Renewable energy and climate change," *Renew. Energy Environ. Sustain.*, vol. 6, 2021, [Online]. Available: https://doi.org/10.1051/rees/2021004
[12] N. A. Pambudi *et al.*, "Renewable Energy in Indonesia: Current Status, Potential, and Future Development," *Sustainability*, vol. 15, no. 3, 2023, doi: 10.3390/su15032342.
[13] V. S. Arutyunov and G. V Lisichkin, "Energy resources of the 21st century: problems and forecasts. Can renewable energy sources replace fossil fuels?," *Russian Chemical Reviews*, vol. 86, no. 8, pp. 777–804, Aug. 2017, doi: 10.1070/rcr4723.
[14] M. Liu *et al.*, "Perspiration permeable, textile embeddable microfluidic sweat sensor," *Biosens Bioelectron*, vol. 237, p. 115504, 2023, doi: https://doi.org/10.1016/j.bios.2023.115504.
[15] J. Gao, L. Dai, W. Zhang, S. Huang, and X. Wu, "Multi-Interval Efficiency Design Optimization for Permanent Magnet Synchronous Generators Used in Hybrid Electric Special Vehicles," *IEEE Transactions on Industrial Electronics*, vol. 68, no. 6, pp. 4646–4656, 2021, doi: 10.1109/TIE.2020.2988222.
[16] X. Dai *et al.*, "A hybrid energy harvesting system for self-powered applications in shared bicycles," *Sustainable Energy Technologies and Assessments*, vol. 51, p. 101891, 2022, doi: https://doi.org/10.1016/j.seta.2021.101891.
[17] A. Buonomano, "Building to Vehicle to Building concept: A comprehensive parametric and sensitivity analysis for decision making aims," *Appl Energy*, vol. 261, p. 114077, 2020, doi: https://doi.org/10.1016/j.apenergy.2019.114077.
[18] S. M. Hosseini, M. Soleymani, S. Kelouwani, and A. A. Amamou, "Energy Recovery and Energy Harvesting in Electric and Fuel Cell Vehicles, a Review of Recent Advances," *IEEE Access*, vol. 11, pp. 83107–83135, 2023, doi: 10.1109/ACCESS.2023.3301329.
[19] L. Sun, L. He, Z. Li, F. Zhong, B. Yu, and J. Lin, "An inclined pedal type piezoelectric energy harvester for pedestrian flow and vehicle safety monitoring," *Sustainable Energy Technologies and Assessments*, vol. 63, p. 103646, 2024, doi: https://doi.org/10.1016/j.seta.2024.103646.
[20] E. S. Wirateruna and A. F. A. Millenia, "Design of MPPT PV using Particle Swarm Optimization Algorithm under Partial Shading Condition," *International Journal of Artificial Intelligence & Robotics (IJAIR)*, vol. 4, no. 1, pp. 24–30, May 2022, doi: 10.25139/ijair.v4i1.4327.
[21] E. S. Wirateruna, M. J. Afroni, and F. Badri, "Design of Maximum Power Point Tracking Photovoltaic System Based on Incremental Conductance Algorithm using Arduino Uno and Boost Converter ," *Applied Technology and Computing Science Journal*, vol. 4, no. 2, pp. 101–112, 2022.
[22] J. Bhookya, M. Vijaya Kumar, J. Ravi Kumar, and A. Seshagiri Rao, "Implementation of PID controller for liquid level system using mGWO and integration of IoT application," *J Ind Inf Integr*, vol. 28, p. 100368, 2022, doi: https://doi.org/10.1016/j.jii.2022.100368.
[23] M. Huba and D. Vrancic, "Performance Portrait Method: An Intelligent PID Controller Design Based on a Database of Relevant Systems Behaviors," *Sensors*, vol. 22, no. 10, 2022, doi: 10.3390/s22103753.
[24] A. Noordin, M. A. Mohd Basri, and Z. Mohamed, "Real-Time Implementation of an Adaptive PID Controller for the Quadrotor MAV Embedded Flight Control System," *Aerospace*, vol. 10, no. 1, 2023, doi: 10.3390/aerospace10010059.
[25] T. Shuprajhaa, S. K. Sujit, and K. Srinivasan, "Reinforcement learning based adaptive PID controller design for control of linear/nonlinear unstable processes," *Appl Soft Comput*, vol. 128, p. 109450, 2022, doi: https://doi.org/10.1016/j.asoc.2022.109450.